Enhanced particle flux due to localized divertor MHD instability in DIII-D tokamak

H.Q. Wang, J.G. Watkins[a], H.Y. Guo, A.W. Leonard, D.M. Thomas, A.A. Stepanenko[b], S.I. Krasheninnikov[c]

General Atomics, PO Box 85608, San Diego, CA 92186-5608, USA

[a]*Sandia National Laboratories, PO Box 969, Livermore, CA 94551, USA*

[b]*National Research Nuclear University MEPhI (Moscow Engineering Physics Institute), 115409 Moscow, Kashirskoe highway, Russia*

[c]*Department of Mechanical and Aerospace Engineering, University of California, San Diego, 9500 Gilman Drive, La Jolla, California 92093, USA*

Abstract

An MHD mode with frequency < 10kHz has been identified near the inner strike point from various diagnostics, i.e. divertor Langmuir probes, magnetics sensors and interferometers, but does not appear in the upstream and core diagnostics. This MHD mode is associated with magnetic oscillations >~ 5G, has a long wavelength in the toroidal direction with toroidal mode number n=1, but is localized in a narrow radial region of a few cm. The mode appears when the outer strike point stays attached and the inner strike point nearly detaches, grows with increasing density, and eventually weakens and vanishes as the outer strike point detaches. This mode results in particle flux an order of magnitude higher than the background plasmas near the inner strike point. The mode characteristics are consistent with the Current-Convective-Instability theory prediction. Initial simulations based on experimental input have found oscillations with similar frequencies but weaker amplitude.

Introduction------One of the critical issues for future fusion reactor-relevant devices is to achieve high performance plasmas with tolerable heat load on the plasma facing components[1]. Therefore, a highly dissipative divertor with a strong temperature gradient along the flux tube, is necessary and understanding the underlying physics is vitally important for the operation of future fusion reactors.

It has recently been found that between the onset of detachment and complete detachment state, a fluctuating detachment state[2] exists, characterized by strong fluctuations of radiation near the X-point region[3]. It appears that the high density localized in high-field side scrape-off layer (HFSHD) associated with the fluctuating detachment state plays an important role on the pedestal structure and pedestal performance[4,5,6]. For example, the HFSHD could cause significant diffusion-type fueling into the pedestal, lead to significant relative shift between the density and temperature pedestals, and thus strongly affect the pedestal performance[4]. So far, there are several physical mechanisms, such as the ionization-recombination instability[7] and current-convective instability[8], proposed to be responsible for the instability. In the DIII-D tokamak, an MHD mode with long toroidal wavelength, narrow radial range and frequency lower than 10kHz has been found near the inner strike point. The mode frequency and associated high particle flux in the HFS are similar to those observed in AUG and claimed as the ionization-recombination instability. In DIII-D, it is found that the mode has toroidal mode number n=1, produces poloidally localized magnetic perturbations, and initially grows with density but then weakens and disappears as the outer strike point approaches detachment, which is different from the ionization-recombination theory. These mode features and density dependence agree with the prediction of the current-convective instability theory.

Experimental results------Figure 1 shows a typical DIII-D H-mode discharge with 5.5MW NBI heating, 1.3MA plasma current, lower-single null with ion $B\times\nabla B$ toward the lower X-point, outer strike point on the flat target plate and inner strike point at a slanted target. At the pedestal top, the inter-ELM electron temperature measured by the Thomson Scattering system is about 500eV and electron density is about $4.5\times 10^{19}m^{-3}$. Electron temperature as measured by divertor Langmuir probes near the outer strike point is about 40eV, while near the inner strike point, the peak temperature is about 10eV, showing a

strong in-out divertor asymmetry as expected[9]. The D_α emission near the inner strike point (Fig. 1-d) features a quasi-coherent fluctuation with frequency about 5kHz, accompanied by its second harmonic and another weak 3kHz fluctuation. In this discharge, both the density and temperature at the pedestal top are modulated by the ELMs with frequency of about 70Hz.

The oscillation is excited after the ELM crash, grows, saturates for about 10ms and then disappears right before the next ELM crash, but during the saturation phase the frequency is about 5kHz. The fluctuation has also been detected by other diagnostics, such as the divertor Langmuir probes embedded in the tile and magnetic coils near the inner strike point. From the divertor D_α emission, the fluctuation amplitude is much smaller than the ELM but is comparable or much higher than the background level. The fluctuations result in a time-derivate magnetic perturbation about 20G/s, corresponding to a magnetic perturbation about 5G which is comparable to some core MHD activity.

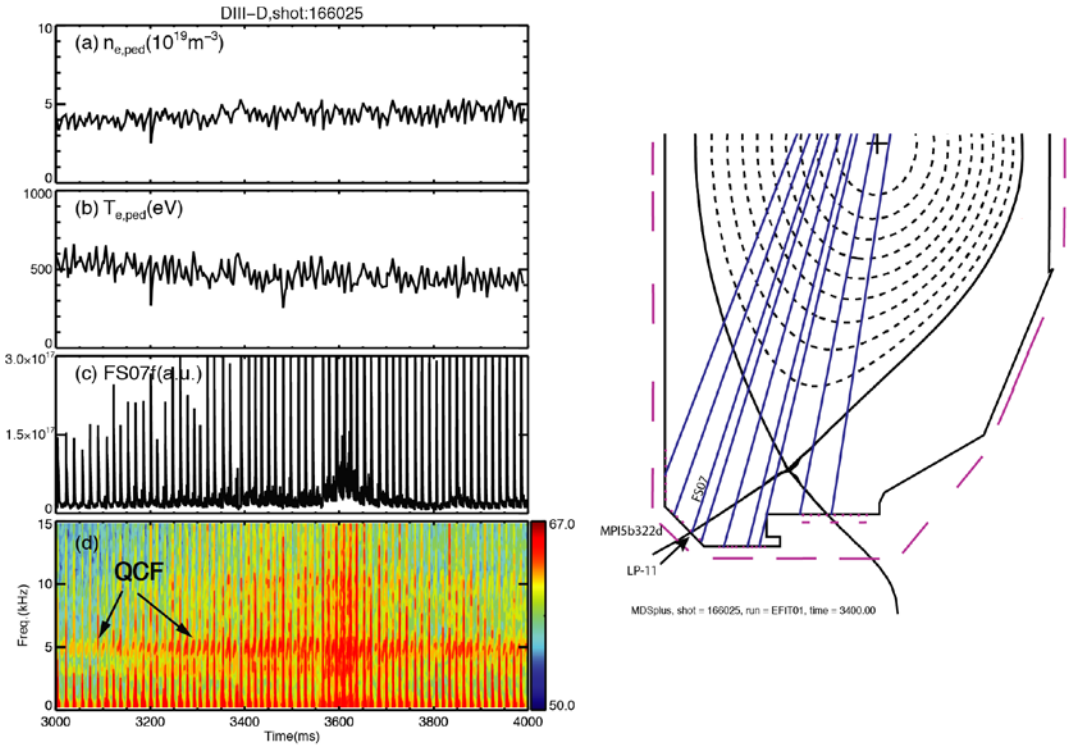

Figure 1. Left: (a) electron density at the pedestal top from TS, (b) electron temperature at the pedestal top from TS, (c) divertor Dα emission from the inner target plate, (d) time-frequency spectrum for the Dα emission indicating the quasi-coherent fluctuations (QCF). Right: typical plasma shape from EFIT

equilibrium reconstruction indicating locations for the divertor D_α emission (FS07), target Langmuir probe (LP-11) and magnetic sensors (MPI5bm322d).

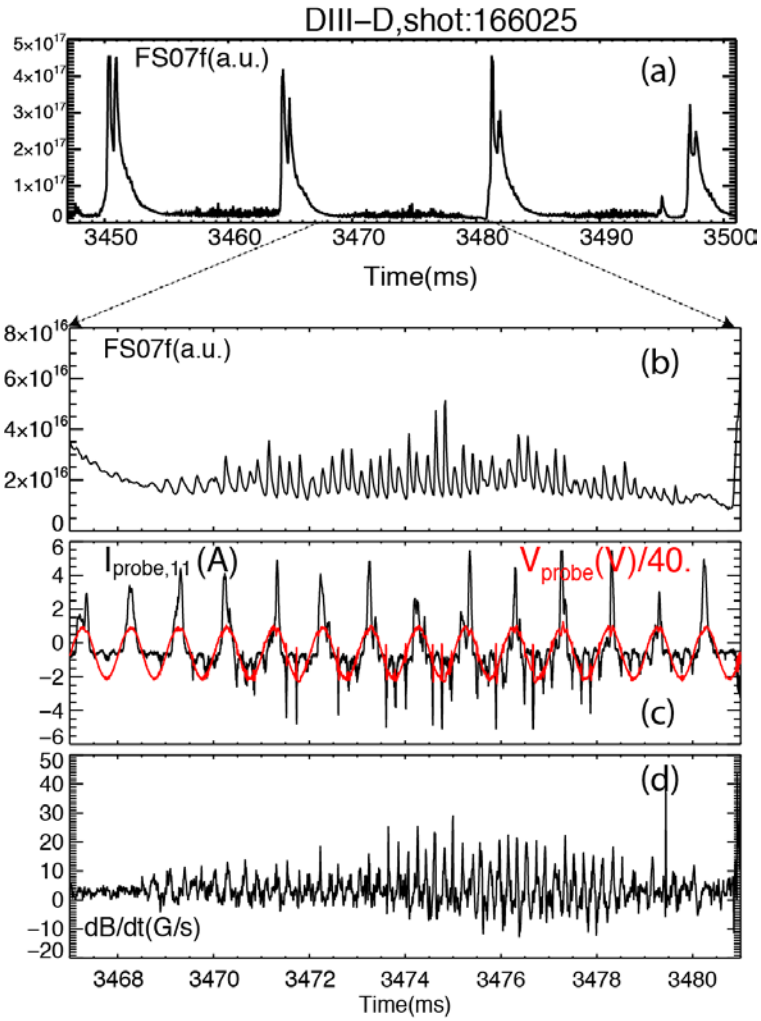

Figure 2. (a) divertor D_α emission from the inner target plate, (b) zoom-in of (a), (c) Langmuir probe current and voltage of probe located near the inner strike point, (d) magnetic perturbation near the inner strike point.

The fluctuations in the probe current strongly correlate with those in the divertor Dα emission and the magnetic perturbations, as shown in Fig. 2e-f and Fig. 3. Although probe current and voltage are digitized at 1MHz, the bias sweep frequency is 1 kHz, much slower than the fluctuations and therefore it is not possible to obtain density, temperature, potential and heat flux, from the fitting I-V characteristics. On the other hand, ion saturation current is measured directly when the probes are biased negatively so particle flux changes at high frequency can be observed directly.

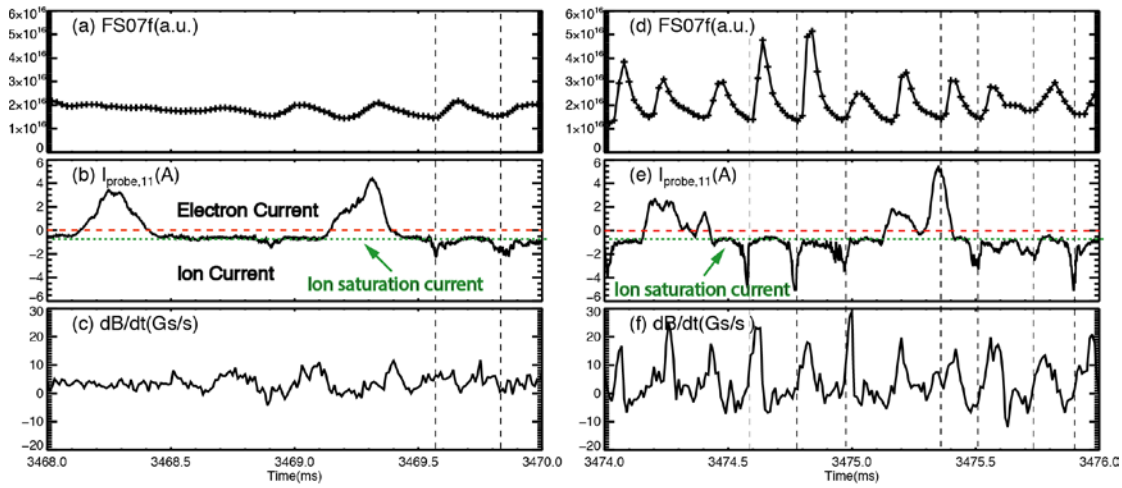

Figure 3. Zoom-in plot of the Fig. 2 for two short time windows: (left column) shortly after ELM crashes when the fluctuations are low, and (right column) later in time when the fluctuations are strong. (a) divertor Dα emission from the inner target plate, (b) Langmuir probe current and voltage of probe located near the inner strike point, (c) magnetic perturbation near the inner strike point. The ion saturation current is clearly indicated by a green line. The dashed vertical lines show times of strong correlation between the magnetic sensors, the floor probe and the Dα spikes and dips in the probe current.

Fig. 3 shows two separate times between ELMs approximately 2 ms in duration that allow direct comparison of the correlation between fluctuations in the ion saturation current (a proxy for particle flux) and other signals. Figs 3-a-c show low level of fluctuations while Fig. 3 d-f, later in time, show higher levels. Vertical dashed lines mark spikes in ion saturation current that also appear in the magnetic sensors and in the divertor D_α signals (albeit with some delay due to toroidal separation). The duration of the spikes in the floor probe (negative) and magnetic signals (positive) is much shorter than in the D_α signals as the later involves a chain of atomic and molecular processes. The spikes shown in the probe ion current direction are an order larger than the background ion saturation current, suggesting high particle fluxes for both ions and electrons are flowing towards the divertor target.

These fluctuations are localized near the inner strike point and are much weaker or non-existent on other floor probes, such as the ones in the inner SOL, private flux region and near the outer strike point, so they are different from some previously characterized low-frequency fluctuations, like the limit-cycle oscillation[10], or the M-mode[11], which has been found in a broad region.

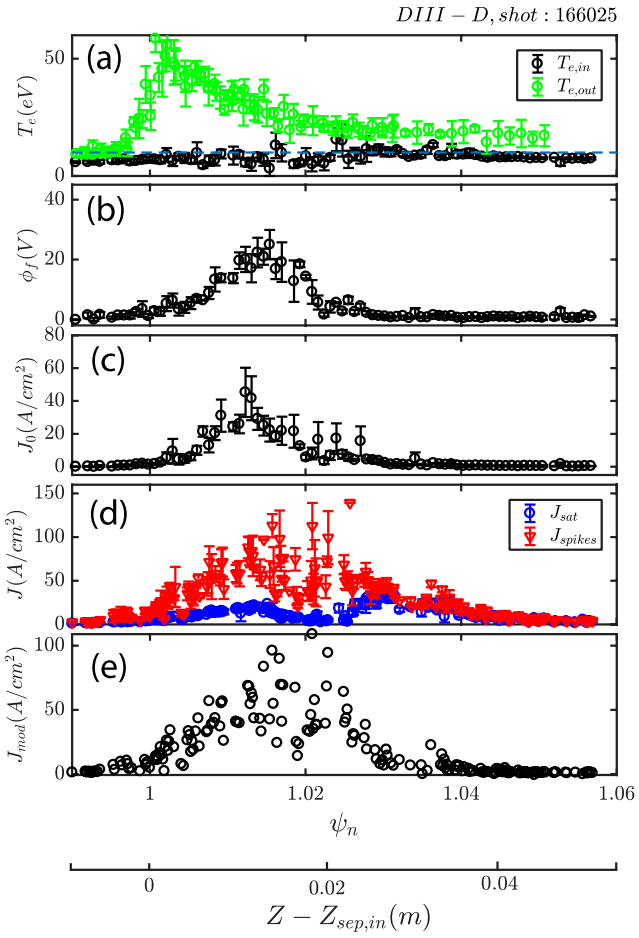

Figure 4. Radial profiles of (a) electron temperature near the outer strike point(green) and inner strike point (black), (b) floating potential, (c) ground current, (d) the background ion saturation current (blue circles), the amplitude of the probe current fluctuations (red triangle), and (e) the mode-only induced probe current. The spikes, background ion saturation current and mode-only induced probe current will be discussed in the context.

The strike point is swept across several fixed floor probes in order to obtain the radial profile of the divertor conditions and the mode spatial characteristics. As can be seen in the Fig. 4, although the electron temperature (Fig. 4a) is low (<10eV) near the inner strike point, both the floating potential (Fig. 4(b)) and ground current (Fig. 4(c)) are still significant near the strike point, which provides the possibility to drive current-related instabilities. We use conditional averaging to separate the current driven by the fluctuations from the background ion saturation current. To do so, we filter out the ELMs (30-99% of the ELM phase), select the ion-saturation part of probe current, separate the

measured points into a series of segments with the typical period of QCF, i.e. 0.2ms, and then pick both the maximum and minimum currents for each segment. The maximum current for each segment corresponds to the background ion saturation current, and the minimum corresponds to the peak of negative spike resulting from the mode. After applying a 5ms median filter for 2s data and mapping the probe locations with the strike points calculated from the EFIT equilibrium reconstruction, as can be seen in Fig. 4(d), the peak particle flux of the mode is an order higher than the background ion saturation current (Fig. 4(d) blue). The ion saturation current profile exhibits a double-peak structure with the second peak ~2.5cm away the inner strike point. By subtracting the background ion flux, the particle flux of the mode could be obtained, i.e. $J_{mod}=J_{spikes}-J_{sat}$, as can be seen in Fig. 4(e). Since several ELM crashes appear during the sweeping and the mode is evolving during the inter-ELM phase, the ion current of the negative spike is fluctuating. The peak current is up to 120A/cm^2 which is about factor 5 times higher than the peak background ion saturation current and about an order higher than the background ion current at the same radial location. In addition, the mode is radially localized to be within 3cm of the strike point with an exponential decay length about 2cm which is close to the SOL heat flux width.

As shown in Fig. 5, the magnetic perturbations related to this mode are only observed near the inner strike point (Fig. 5(a)). The magnetic coils near the outer strike point (Fig. 5(d)), at the inboard midplane (Fig. 5(b)) and near the outboard midplane (Fig. 5(c)) did not detect the mode, although these magnetic sensors do detect other core MHD with higher or lower frequency. This highly poloidally localized characteristic is strongly different from other MHD modes, such as the core tearing mode, Alfven Eigenmodes, which can be detected by the midplane magnetic probes. As can be seen in Fig. 5(e) (f), the cross-spectrum and coherence from the poloidal array of magnetic perturbations show similar features about this fluctuation.

From the magnetic perturbation profiles, it is possible to reconstruct the current oscillation, a full treatment of which requires detailed 2D modeling. For simplicity, if we assume there is a toroidal current-sheet with the SOL width wide and poloidal leg length long, we can obtain a similar magnetic perturbation profile. The required amplitude of current is about 300A, which is similar to the divertor ground current and same order of

the plasma ion saturation current. The temperature difference between the inner and outer divertors could induce the thermal-electric current, which may explain part of the SOL current, especially in the SOL region. The charge separation from the magnetic drift and diamagnetic drift would result in the Pfirsch-Schluter current[12] which could be important in the cold plasma region, i.e., in the private flux region, where the thermal electric current[13] would be weak.

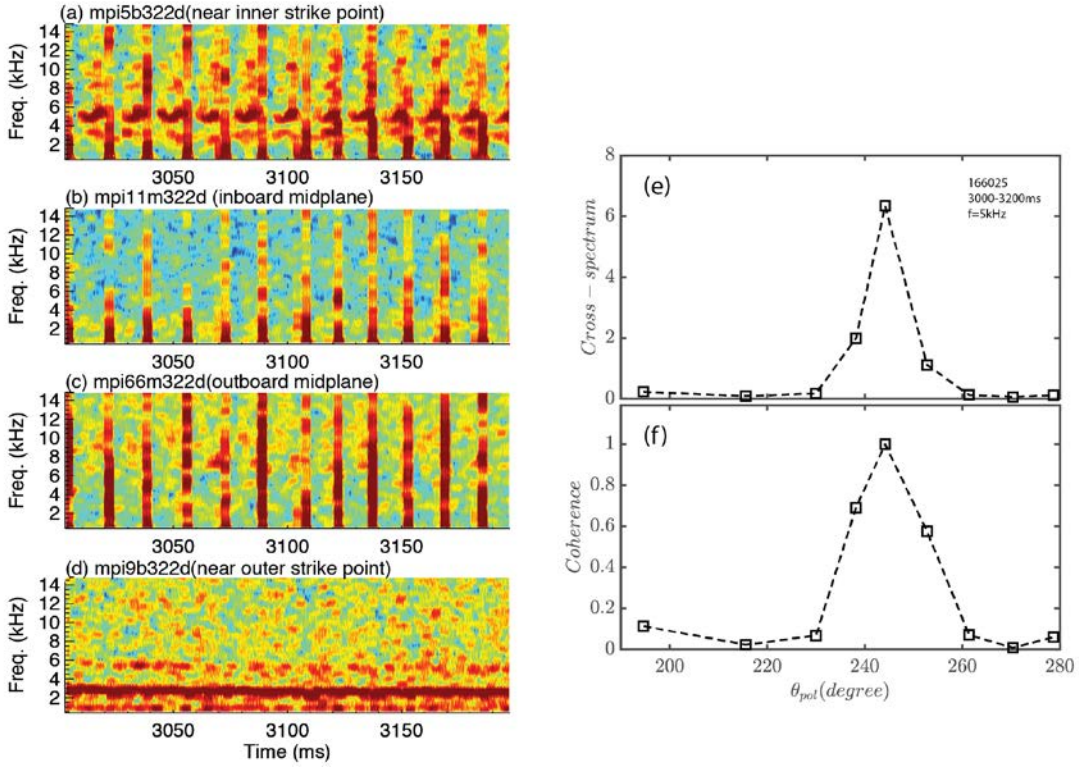

Figure 5. Magnetic perturbation from the magnetic pick-up sensors (a) near the inner strike point, (b) inboard midplane, (c) outboard midplane, (d) near the outer strike point. The fluctuation level (e) and coherence (f) from the magnetic sensors in different poloidal locations. 0 degree is the HFS midplane, 250 degree is near the inner strike point.

Since the mode exhibits very localized characteristics in poloidal space, it is difficult to obtain the poloidal mode number. Instead, its toroidal mode number could be obtained principally from several toroidal separated magnetic sensors. Unfortunately, for the cases we discussed in Fig. 5, the toroidal separated magnetic sensors were not available. Subsequent shots (at a different power and plasma current) with the requisite arrays were therefore used to obtain the toroidal mode number information. As can be seen in Fig. 6,

for this shot, the mode exhibits a toroidal mode number n=1, while its second harmonic has a toroidal mode number n=2. In this discharge, the fluctuations exhibit a frequency about 3kHz. The frequency changes may be due to the different powers and/or plasma current, which will require further systematical datasets to understand.

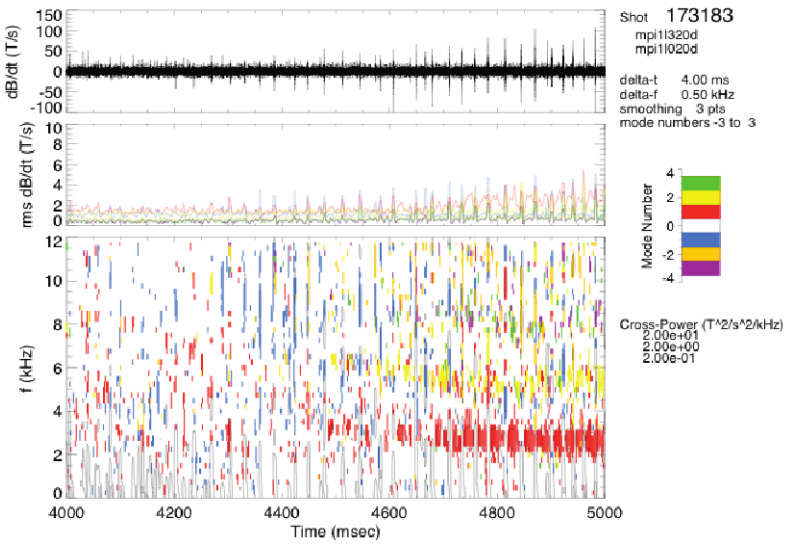

Figure 6. Toroidal mode number from the two toroidally separated magnetic sensors.

The poloidally-localized nature of the mode was also confirmed by differences in the line-integrated density measurements from the interferometer. As shown in Fig. 7, the fluctuations exhibit several harmonics with base frequency about 3kHz and only appear in the V1 chord which goes through the inner strike point (Fig. 7(a). They are not detectable in the V2 (outer SOL, Fig. 7(b)), V3 (outer SOL, Fig. 7(c)) and R0 chords (outer midplane, Fig. 7(d)). It is also interesting to see that the line-integrated density of V1 is typically higher than that in the other chords, suggesting that there is higher density in the inner strike point, consistent with a high-field side high density front. Such high-field side high density is consistent with a divertor in-out asymmetry driven by ExB drift in the divertor region[4]. Consistent with this picture, in reversed B_T plasmas with ion magnetic drift away from the main X-point, such a difference of the line-integrated density between different chords is much smaller.

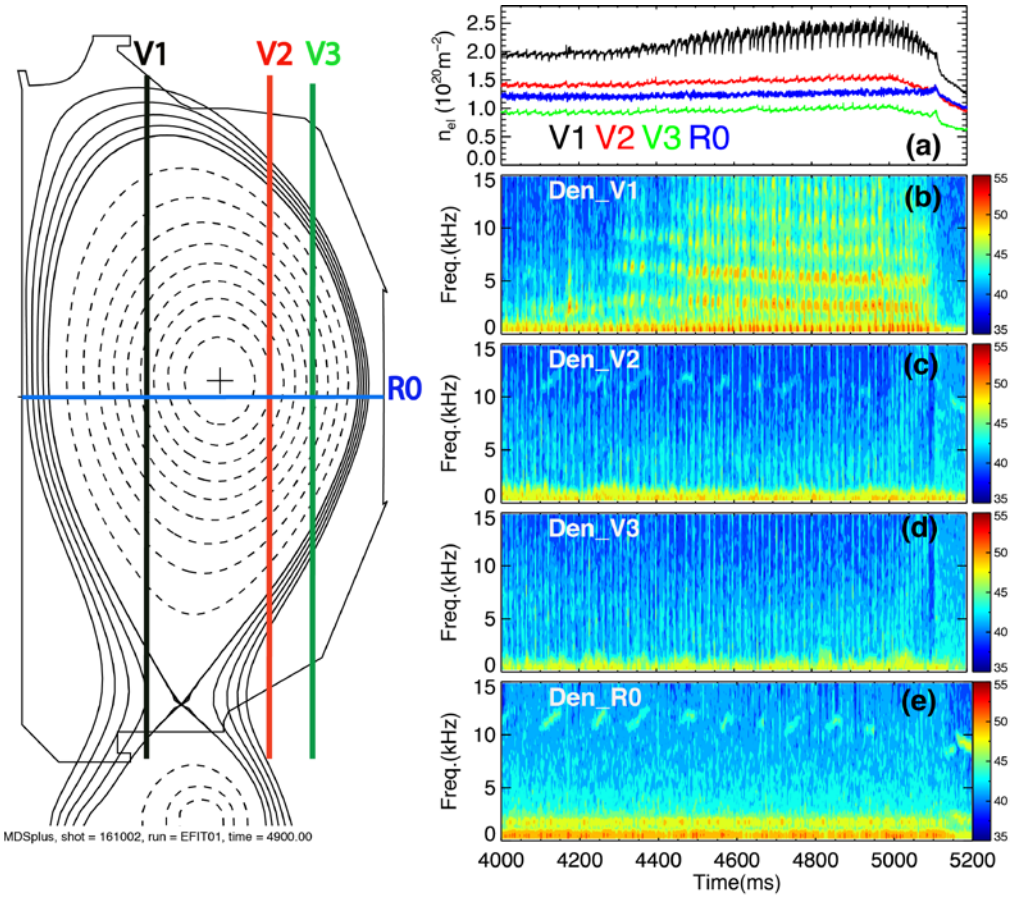

Figure 7. Left: the plasma equilibrium and the different chords of the interferometer. Right: (a) the line-integrated density, time-frequency spectrum of the line-integrated density from different chords (b) V1 (black), through the inner divertor, (c) V2 (red), through the outer SOL, (d) V3 (green), through the LFS, (e) R0 (blue), horizontal chord.

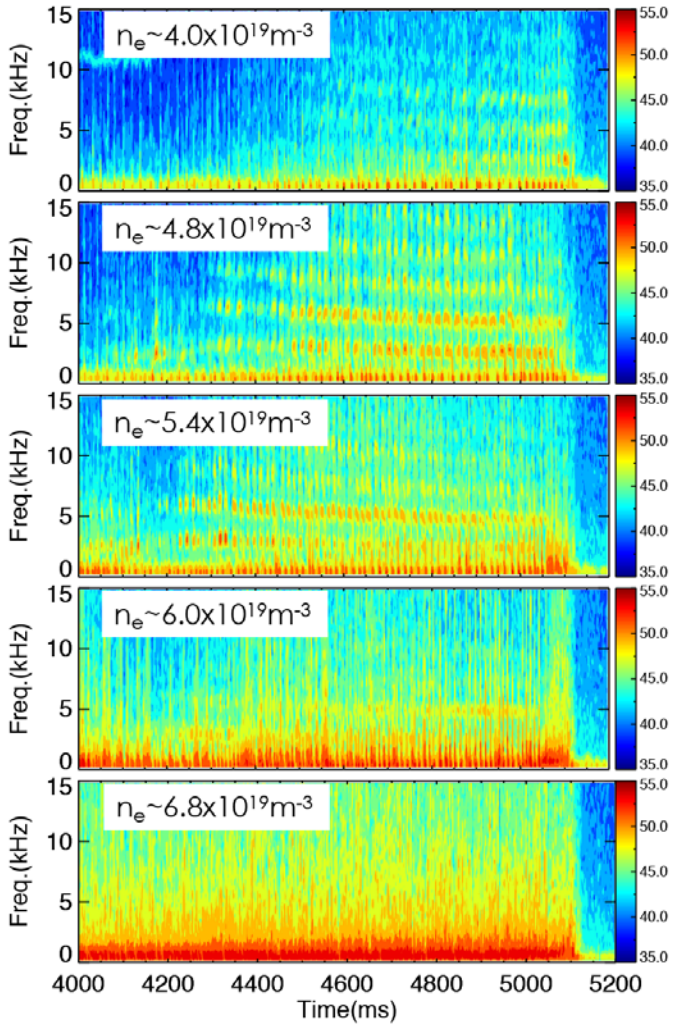

Figure 8. Time-frequency spectrum of the V1 chord line-integrated density for different line-averaged densities. Line-averaged density n_e~4×10^{19}m^{-3} corresponds to attachment (Te>10eV) near both inner and outer divertors; 4.8×10^{19}m^{-}3<ne<6.0×10^{19}m^{-3} corresponds to high-recycling (Te<10eV) in inner divertor and attached in outer divertors; ne~6.8×10^{19}m^{-3} corresponds to well detachment for both inner and outer divertors with Te <2eV.

This fluctuation localized near the inner divertor changes with the divertor conditions. As shown in Fig. 8, as the plasma density is scanned by increasing the gas puffing shot by shot, the fluctuations are very weak at low density when both inner and outer divertor attachment, then enhanced at the middle density with inner strike point at low temperature, become weaker at higher density and disappear at the highest density with both divertor leg detachment. We note that increasing the line-average density only decreases the mode frequency by about 10%.

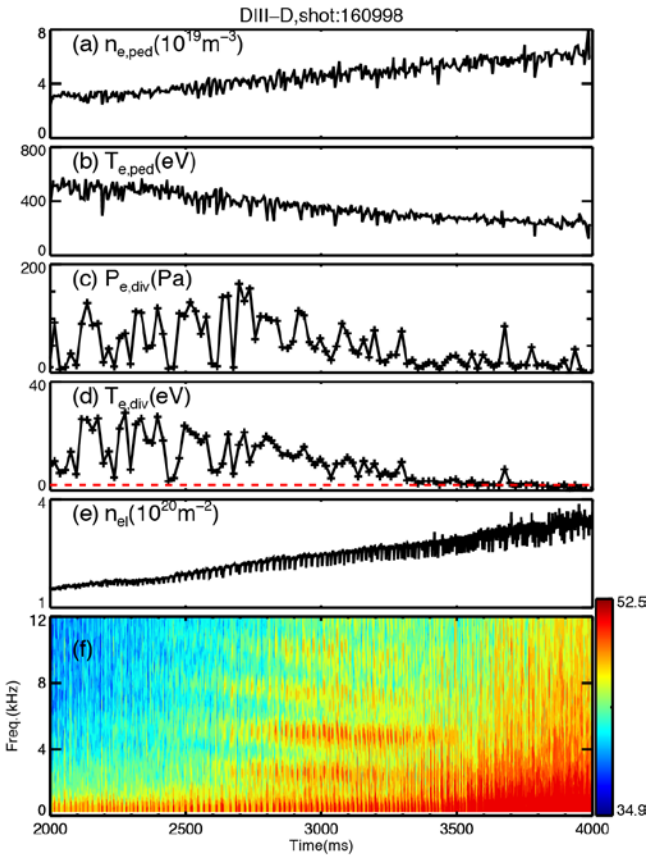

Figure 9. (a) electron density at the pedestal top, (b) electron temperature at the pedestal top, (c) electron pressure near the inner strike point, (d) electron temperature near the inner strike point, (e) line-integrated density, (f) time-frequency spectrum for the line-integrated density.

Such a relationship between this fluctuation and the inner divertor conditions was confirmed by a density ramp-up detachment discharge (Fig. 9). In this case the inner strike point was fixed near the V1 interferometer and the divertor Thomson Scattering. As density increases, both the pedestal electron temperature (Fig. 9(b)) and divertor electron temperature (Fig. 9(d)) decrease, while the fluctuation (Fig. 9(f)) level near the inner strike point increases and then disappears when the inner strike point is well detached with divertor Te lower than 2eV. When the mode is excited, the divertor electron pressure starts to go down. The frequency stays nearly constant even as both pedestal and divertor temperature are changed significantly.

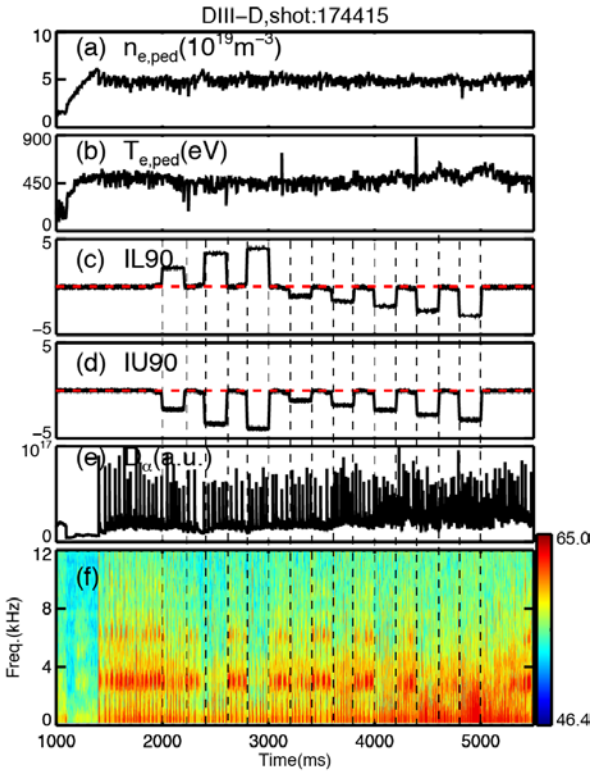

Figure 10. (a) electron density at the pedestal top, (b) electron temperature at the pedestal top, (c) RMP I coil current at lower space, (d) RMP I coil current at upper space, (e) divertor Dα emission, (f) time-frequency spectrum of (e).

This fluctuation could be mitigated by the external RMP[14] coils, as shown in Fig. 10. As the RMP coils are turned on, the mode is suppressed, while when the RMP coils are turned off, the mode appears again. When the RMP coil current is high enough, the mode was significantly suppressed. The RMP could strongly affect the divertor plasma, such as increasing the detachment onset density or inducing potential lobes near the target plate or changing the magnetic geometry near the plate, which both could strongly affect the fluctuation amplitude[14].

Discussion and Initial modeling

Two main physical mechanisms are proposed to explain the quasi-coherent fluctuations observed in the experiment. One is about the ionization-recombination instability. However, DIII-D experiments find that the fluctuations associate with finite

toroidal mode number n=1 which is different from the prediction that detachment instability should associate with global oscillation like n=0.

Another physical mechanism is about the current-convective instability, arising partly due to the in-out diverter asymmetry[9]. In the favorable Bt direction with ion B×∇B directed toward the main X-point, divertor drifts move particles from outer strike point to inner strike point and cools down the inner divertor. Such temperature difference between the inner and outer diverter could result in strong difference in the local plasma current and the potential. As shown in Fig. 4, this SOL current with narrow radial region is the same order as the ion saturation current $j_s = en_eC_s$ and the core plasma current density. The low temperature and high current density could lead to strong parallel electric field near the inner divertor leg. Along with the inhomogeneity of the electric conductivity, this could provide certain free energy to drive some instability, such as the rippling instability[15,16,17] or current-convective instability (CCI)[8,18]. The linear growth rate of the rippling mode is derived based on local theory[17]:

$$\gamma = j_\parallel \eta' (k_\perp / k_\parallel B) - k_\parallel^2 \kappa_\parallel \qquad (1)$$

where $j_{//}$ is parallel current, η is the Spitzer resistivity, $k_\perp$ is the perpendicular wavenumber, $k_\parallel$ is the parallel wavenumber, B is the magnetic field and $\kappa_\parallel$is the parallel thermal conductivity. Significant current density and resistivity gradient are required to destabilize the mode with typically long parallel wavelength and narrow perpendicular width, which is consistent with the experimentally observed strong poloidal localization and low toroidal mode number shown in Fig.4, 5 and 6. High temperature with strong thermal conduction would significantly stabilize the mode, thus the CCI can only occur at the cold plasma region with low temperature, especially Te lower than 10eV, like conditions at the inner divertor region. It is also noted that, when the inner and outer divertor are both well detached, the divertor/SOL current is significantly reduced and thus the CCI is strongly stabilized. These features are consistent with experimental observations shown in Fig.8 and 9.

A simple simulation based on the CCI physical model has been applied to ASDEX-Upgrade-like conditions and shows frequency spectra of turbulent plasma oscillations similar to that in the experimental observations[19]. Similar simulations have also been employed for DIII-D conditions with similar upstream plasma parameters, magnetic field,

magnetic shape, downstream plasma conditions and so on[20]. The simulation makes a series of simplifying assumptions, such as neglecting the convective part of parallel electron heat flux, curvature of the magnetic field lines, warm ions, electromagnetic effects and neutral friction, and assuming homogeneous density profile[20]. The simulation solves the vorticity and electron equations in the framework of the BOUT++ code. The frequency spectra of the parallel current fluctuations at the inner strike point is shown in Fig. 11 and contains strong components with frequency near 2, 5, 11 kHz similar to those experimentally observed in DIII-D experiment. However, the amplitude of the simulated fluctuation is about two orders smaller than those in the experiment. Such discrepancy between simulation and experimental observation could be due to several missing physical terms such as the parallel plasma convection, curvature effects, interchange drive, density effects and electromagnetic effects. More details about the modeling can be found in the recent papers[20]. In future work, more comparison of the simulation incorporating these physical effects and experimental results will be performed to further understand the physical mechanisms related to the divertor detachment.

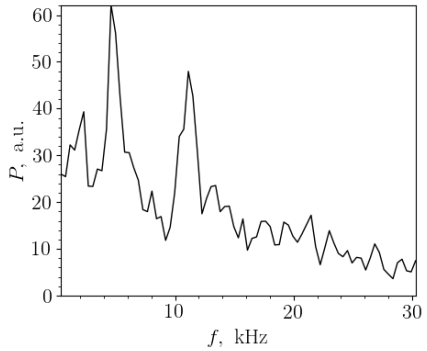

Figure 11. The frequency spectrum of parallel current oscillations at the ISP for the BOUT++ modeling case with $(T_e)_{max}$ = 25 eV.

Summary------ A low-frequency mode has been detected by several divertor diagnostics near the inner strike point but not near the outer strike point or in the upstream and core diagnostics. This is qualitatively consistent with the prediction of current-interchange instability including: (1) the mode is highly localized in narrow radial region within several cm as the order of density or heat flux SOL width; (2) the mode associates with long wavelength along the toroidal direction with mode number n=1 and about 5G magnetic

perturbations, which is at the similar amplitude of magnetic perturbation resulting from the divertor plasma current; (3) the mode is strongly correlates with the inboard divertor conditions. Once the divertor plasma pressure is dissipated, this mode is excited. As increasing the density, it is enhanced firstly, then becomes weaker and finally disappears as the outer strike point approaching detachment. Such experimental observations are consistent with the CCI theory prediction, although the initial modeling still has some discrepancy matching the experimental observations. In experiment, this mode could result in an order of magnitude higher particle flux than the background plasmas near the inner strike point, and also higher recycling flux, both which could potentially affect the divertor conditions and plasma fueling which mainly contributed from the divertor recycling. For the future tokamak-like fusion reactors, high plasma performance with high density, low heat flux toward divertor target and low temperature with Te < 10eV near the divertor plate are required for the steady-state operation, which would possibly enhance the current-convective instability, thus result in giant and uncontrollable divertor oscillations.

Acknowledgement

Author H.Q. Wang would like to thank Dr. J.A. Boedo for very useful discussions. This work is supported by the U.S. Department of Energy under DE-FC02-04ER54698, DE-AC05-06OR23100, DE-FG02-04ER54739 and DE-AC04-94AL85000 and General Atomics Postdoctoral Research Participation Program administered by ORAU.

Reference

[1] A. Loarte, B. Lipschultz, A.S. Kukushkin, G.F. Matthews, P.C. Stangeby, N. Asakura, G.F. Counsell, G. Federici, A. Kallenbach, K. Krieger, A. Mahdavi, V. Philipps, D. Reiter, J. Roth, J. Strachan, D. Whyte, R. Doerner, T. Eich, W. Fundamenski, A. Herrmann, M. Fenstermacher, P. Ghendrih, M. Groth, A. Kirschner, S. Konoshima, B. LaBombard, P. Lang, A.W. Leonard, P. Monier-Garbet, R. Neu, H. Pacher, B. Pegourie, R.A. Pitts, S. Takamura, J. Terry, E. Tsitrone, the I.S. Layer, and D. Group, Nucl. Fusion **47**, S203 (2007).

[2] S. Potzel, M. Wischmeier, M. Bernert, R. Dux, H.W. Müller, A. Scarabosio, and the A.U. Team, Nucl. Fusion **54**, 013001 (2014).

[3] S. Potzel, M. Wischmeier, M. Bernert, R. Dux, H.W. Müller, and A. Scarabosio, J. Nucl. Mater. **438**, 285 (2013).

[4] F. Reimold, M. Wischmeier, S. Potzel, L. Guimarais, D. Reiter, M. Bernert, M. Dunne, and T. Lunt, Nucl. Mater. Energy (2017).

[5] M.G. Dunne, S. Potzel, F. Reimold, M. Wischmeier, E. Wolfrum, L. Frassinetti, M. Beurskens, P. Bilkova, M. Cavedon, R Fischer, B. Kurzan, F.M. Laggner, R.M. McDermott, G. Tardini, E. Trier, E. Viezzer, M. Willensdorfer, T.Euro.M. Team, and T.A.-U. Team, Plasma Phys. Control. Fusion **59**, 014017 (2017).

[6] E. Wolfrum, M. Beurskens, M.G. Dunne, L. Frassinetti, X. Gao, C. Giroud, J. Hughes, T. Lunt, R. Maingi, T. Osborne, M. Reinke, and H. Urano, Nucl. Mater. Energy **12**, 18 (2017).

[7] P. Manz, S. Potzel, F. Reimold, M. Wischmeier, and A.U. Team, Nucl. Mater. Energy **12**, 1152 (2017).

[8] S.I. Krasheninnikov and A.I. Smolyakov, Phys. Plasmas **23**, 092505 (2016).

[9] A.W. Leonard, Plasma Phys. Control. Fusion **60**, 044001 (2018).

[10] H.Q. Wang, G.S. Xu, H.Y. Guo, B.N. Wan, V. Naulin, S.Y. Ding, N. Yan, W. Zhang, L. Wang, S.C. Liu, R. Chen, L.M. Shao, H. Xiong, P. Liu, M. Jiang, and G.-N. Luo, Nucl. Fusion **52**, 123011 (2012).

[11] E.R. Solano, N. Vianello, E. Delabie, J.C. Hillesheim, P. Buratti, D. Réfy, I. Balboa, A. Boboc, R. Coelho, B. Sieglin, S. Silburn, P. Drewelow, S. Devaux, D. Dodt, A. Figueiredo, L. Frassinetti, S. Marsen, L. Meneses, C.F. Maggi, J. Morris, S. Gerasimov, M. Baruzzo, M. Stamp, D. Grist, I. Nunes, F. Rimini, S. Schmuck, I. Lupelli, and C.S. and, Nucl. Fusion **57**, 022021 (2016).

[12] M.J. Schaffer, A.V. Chankin, H.Y. Guo, G.F. Matthews, and R. Monk, Nucl. Fusion **37**, 83 (1997).

[13] G.M. Staebler and F.L. Hinton, Nucl. Fusion **29**, 1820 (1989).

[14] A.R. Briesemeister, J.-W. Ahn, J.M. Canik, M.E. Fenstermacher, H. Frerichs, C.J. Lasnier, J.D. Lore, A.W. Leonard, M.A. Makowski, A.G. McLean, W.H. Meyer, O. Schmitz, M.W. Shafer, E.A. Unterberg, H.Q. Wang, and J.G. Watkins, Nucl. Fusion **57**, 076038 (2017).

[15] H.P. Furth, J. Killeen, and M.N. Rosenbluth, Phys. Fluids **6**, 459 (1963).

[16] B.A. Carreras, P.W. Gaffney, H.R. Hicks, and J.D. Callan, Phys. Fluids **25**, 1231 (1982).

[17] A.B. Hassam and J.F. Drake, Phys. Fluids **26**, 133 (1983).

[18] A.A. Stepanenko and S.I. Krasheninnikov, Phys. Plasmas (201801).
[19] A.A. Stepanenko and S.I. Krasheninnikov, Phys. Plasmas **25**, 012305 (2018).
[20] A.A. Stepanenko, H.Q. Wang, and S.I. Krasheninnikov, Plasma Phys. Rep. (2019).